



# The kinetics of the reaction of majorite plus ferropericlasite to ringwoodite: Implications for mantle upwellings crossing the 660 km discontinuity

D.P. Dobson<sup>a,\*</sup>, E. Mariani<sup>b</sup>

<sup>a</sup> Department of Earth Sciences, University College London, Gower Street, London WC1E 6BT, UK

<sup>b</sup> Department of Earth, Ocean and Ecological Sciences, University of Liverpool, Jane Herdman Building, 4 Brownlow Street, Liverpool L69 3GP, UK



## ARTICLE INFO

### Article history:

Received 31 January 2014

Received in revised form 6 August 2014

Accepted 8 October 2014

Available online 24 October 2014

Editor: T. Elliott

### Keywords:

660 km discontinuity

reaction kinetics

perovskite

ringwoodite

majorite

## ABSTRACT

We have measured the kinetics of reaction between MgO and majoritic garnet at 20 GPa and 1773–2123 K as a proxy for the reaction between perovskite and ferropericlasite during mantle upwelling across the 660 km seismic discontinuity. Ringwoodite forms a layer between MgO and garnet and, in the case of aluminous garnets the interface between ringwoodite and garnet develops a fingering instability resulting in a complex intergrowth at this interface. By contrast, the MgO–ringwoodite interface is always planar for an initial planar MgO–garnet interface. Two thicknesses are therefore defined; (1) a layer thickness,  $X_1$ , which is the maximum thickness of ringwoodite which forms a plane-parallel bounded layer next to the MgO, and (2) an interface thickness,  $X_2$ , which is the maximum extent of the intergrowth region away from the ringwoodite layer. The growth of both of these regions can be described by apparent rate constants,  $k_i$ , which are Arrhenius with  $\ln(k_1^0) = -6.36 \pm 0.25 \text{ m}^2/\text{s}$  and  $E_1 = 456 \pm 40 \text{ kJ/mol}$  for the ringwoodite layer, and  $\ln(k_2^0) = -9.2 \pm 3.3 \text{ m}^2/\text{s}$  and  $E_2 = 371 \pm 53 \text{ kJ/mol}$  for the intergrowth region. The fingering instability is caused by the incompatibility of aluminium in ringwoodite and its low chemical diffusivity in garnet which results in an increase of surface area at the ringwoodite–garnet interface to minimise the aluminium concentration at the interface. The intergrowth region contains a fine-grained mixture of ringwoodite and garnet which coarsens very slowly with time. This might result in a transient weakening of upwelling regions of mantle just above the 660 km seismic discontinuity allowing some viscous decoupling between the upper and lower mantle.

© 2014 The Authors. Published by Elsevier B.V. This is an open access article under the CC BY license (<http://creativecommons.org/licenses/by/3.0/>).

## 1. Introduction

The grain size of the lower-mantle is an important, but poorly constrained, geophysical parameter, controlling, among other things, its viscosity (in diffusion creep) and the relative importance of radiative versus lattice thermal conduction. The grain size of the lower mantle was initially set by primary crystallisation from a deep magma ocean and has subsequently been modified by competing processes of grain growth and recrystallisation. Grain growth occurs in order to minimise the surface energy of the system whereas recrystallisation occurs in response to deformation-induced damage to grains or phase transitions as convecting mantle material passes between regions where different phases are thermodynamically stable (e.g. [Solomatov and Reese, 2008](#)). The 660 km seismic discontinuity is particularly

\* Corresponding author.

E-mail address: [d.dobson@ucl.ac.uk](mailto:d.dobson@ucl.ac.uk) (D.P. Dobson).

important in this respect because, unlike most of the upper-mantle phase transitions, the ringwoodite  $\leftrightarrow$  perovskite + ferropericlasite post-spinel reaction is a dissociation reaction where the kinetics of the prograde and retrograde reactions are fundamentally different. The prograde reaction (during subduction and mantle downwelling) has been previously studied since it has significant implications for the cessation of deep seismicity in subducting slabs, as well as for their grain size and strength ([Kubo et al., 2000, 2002](#); [Yamazaki et al., 1996, 2009](#)). The dissociation of ringwoodite  $[(\text{Mg,Fe})_2\text{SiO}_4]$  requires local diffusion of chemical species to form new grains of the equilibrium phases, perovskite  $[(\text{Mg,Fe})\text{SiO}_3]$  and ferropericlasite  $[(\text{Mg,Fe})\text{O}]$ . This diffusion can be on a very short length-scale ( $<1 \mu\text{m}$ ) and the reaction progresses on geologically short timescales but results in fine-grained intergrowths of perovskite and ferropericlasite (e.g. [Ito and Takahashi, 1989](#)). Hydrostatic experiments that studied the growth kinetics of the perovskite–ferropericlasite assemblage have shown that this is sluggish ([Yamazaki et al., 1996](#)), resulting in an inferred lower-mantle grain size of  $<100 \mu\text{m}$ . This conclusion has been

questioned by subsequent studies: (1) Solomatov et al. (2002) argue that the experiments were not sufficiently long to evaluate grain growth kinetics beyond the transient effects due to textural re-equilibration of lamellar intergrowths produced by the eutectoid post-spinel reaction; (2) experiments in which the analogue system  $\text{Mg}_2\text{SiO}_4$  olivine plus MgO was deformed in superplastic creep (Hiraga et al., 2010) suggest that deformation might enhance grain growth through a process of grain-boundary sliding and grain switching; (3) it has also been suggested, on the basis of (i) the temperature of the plume source region, (ii) the kinetics of grain growth from an early magma ocean and (iii) seismic tomographic imaging of wide plume roots, that deep-mantle plumes might have a significantly larger grain size than the ambient lower mantle (Solomatov, 1996; Korenaga, 2005).

The retrograde reaction, from the lower-mantle assemblage perovskite + ferropericlase to the transition-zone assemblage ringwoodite + garnet (during mantle upwelling) requires diffusion on a much larger length-scale as macroscopic grains of perovskite and ferropericlase must recombine to form ringwoodite. In this case, the reaction kinetics will be controlled by diffusion of chemical components through the layer of ringwoodite which forms at the interface between individual grains of ferropericlase and the surrounding  $(\text{Mg,Fe})(\text{Al,Si})\text{O}_3$ . This should result in a reaction rate which is strongly sensitive to the grain size of the lower mantle and, if the metastable ferropericlase + majoritic garnet assemblage has different seismic properties from the equilibrium ringwoodite + garnet assemblage, the position and form of the 660 km discontinuity might contain useful information regarding the grain size of the lower mantle. A recent study (Shimojuku et al., 2014) investigated the kinetics of the reaction of perovskite plus periclase to ringwoodite in the simple Mg–Si–O system and found the kinetics to be sufficiently fast that no discernable shallowing of the 660 km seismic discontinuity should occur at plumes due to the kinetics of reaction.

Reactions around 660 km depth in the Earth are complicated by the fact that the mantle is not a simple MgO–FeO– $\text{SiO}_2$  ternary system; in particular the  $\text{Al}_2\text{O}_3$  component is strongly soluble in  $\text{MgSiO}_3$  perovskite (and garnet) but not in ringwoodite (e.g. Hirose, 2002). The composition of the mantle (in FeO–MgO– $\text{Al}_2\text{O}_3$ – $\text{SiO}_2$  space) falls between the ringwoodite  $(\text{Mg,Fe})_2\text{SiO}_4$  and perovskite  $(\text{Mg,Fe})(\text{Al,Si})\text{O}_3$  compositions, resulting in an equilibrium lower-mantle assemblage of perovskite plus ferropericlase and a transition-zone assemblage of ringwoodite plus garnet. Upper-mantle composition  $(\text{Mg}_{0.9}\text{Fe}_{0.1})_2\text{SiO}_4$  ringwoodite decomposes to perovskite plus ferropericlase at 23.5 GPa and 1873 K, giving rise to the 660 km seismic discontinuity and the width of the three-phase loop is narrow, corresponding to less than 4 km in the mantle (Ito and Takahashi, 1989). By contrast, for more enriched compositions (e.g. pyrolite) and at higher temperatures appropriate to mantle plumes the equilibrium phase assemblage changes from ringwoodite plus garnet to ferropericlase plus garnet and, finally, ferropericlase plus perovskite with increasing pressure (e.g., Hirose, 2002; Akaogi et al., 2002; Nishiyama et al., 2004). This would result, in upwelling regions, in majoritic garnet being progressively exsolved from perovskite starting around 730 km depth until, at 660 km, the perovskite is completely transformed into garnet. Thus, as ringwoodite becomes stable at pressures below 23.5 GPa the metastable starting assemblage is majoritic garnet plus ferropericlase. Here we present laboratory experiments to measure the kinetics of the reaction  $\text{MgSiO}_3$  (garnet) +  $\text{MgO} = \text{Mg}_2\text{SiO}_4$  (ringwoodite) in model iron- and alumina-bearing systems.

## 2. Methods

### 2.1. High-pressure experiments

High-pressure experiments were performed in a 1000-ton split-cylinder multi-anvil press at the Bayerisches Geoinstitut using a standard 10/5 cell assembly described elsewhere (e.g. Dobson et al., 2002). Starting materials consisted of plates of single-crystal MgO, cored parallel to the [100] crystallographic direction to 1.2 mm diameter and double polished to a thickness of 100–200  $\mu\text{m}$ . These were packed between powders of different majoritic compositions in a polycrystalline MgO capsule. The axis of the MgO disc was oriented as closely as possible to be coincident with the capsule and furnace axes. The majoritic composition powders comprised a  $(\text{MgSiO}_3)_{0.95}(\text{Al}_2\text{O}_3)_{0.05}$  glass on one side of the MgO disc and a natural San Carlos enstatite of composition  $(\text{Mg}_{0.87}\text{Fe}_{0.08}\text{Ca}_{0.02}\text{Al}_{0.03})(\text{Si}_{0.97}\text{Al}_{0.03})\text{O}_3$  on the other side of the disc. At the pressures of the experiments, these glass and enstatite components rapidly transformed to majorite garnet such that no untransformed material was observed in any experiment, even at the lowest temperature and shortest duration. In most cases the MgO capsule was packed directly into a  $\text{LaCrO}_3$  furnace, resulting in strongly oxidising conditions, but for several experiments an outer Mo foil capsule was added to ensure that the oxygen fugacity was close to assumed lower-mantle values of iron-wüstite minus 2 log units (e.g. Otsuka et al., 2010). No systematic difference in the reaction kinetics was observed between the un-buffered and buffered experiments. Temperature was monitored using W–Re thermocouples inserted co-axially to the furnace with their hot-junctions terminating on a disc of rhenium foil placed between them and the end of the capsule. In all cases the thermocouple junction was within 500  $\mu\text{m}$  of the MgO disc which was as close to the centre of the furnace as possible. The MgO disc was therefore likely to have been 50–100 K hotter than the thermocouple reading: quoted temperatures have not been corrected for this. Loaded cells were stored under low vacuum at 150 °C for 12 h or more prior to high-pressure experiments in order to minimise contamination from adsorbed surface water.

Experiments were performed by first compressing the cell to the pressure of interest (20 GPa) and then heating to the target temperature over a period of 30 min. The final approach to temperature from 1473 K was achieved in <10 min meaning that reaction during this stage was negligible compared to the duration of the experiments. The temperature was maintained for durations of between 30 min and 2 days after which temperature was quenched by cutting power to the furnace. Cells were slowly decompressed and sectioned for analysis, with the furnace axis contained in the plane of the section. Experimental conditions and durations are presented in Table 1.

A further experiment was performed as above but using an alumina-free glass with a composition of  $(\text{Mg}_{0.85}\text{Fe}_{0.1}\text{Ca}_{0.05})\text{SiO}_3$ . This experiment was informative as regards the mechanism of mass transfer across the reaction zone (see below) but it was not used in determining the kinetics of the reaction.

### 2.2. Analysis

Polished samples were analysed by Raman spectroscopy for initial phase identification. The polished surface of the cell was then coated with ~30 nm of carbon and imaged by back-scattered electron (BSE) imaging using a JEOL JSM-6480LV scanning electron microscope (SEM) at University College London at 15 kV accelerating voltage. Line-profiles of chemical composition were measured in the same SEM using Link ISIS software in scanning mode. These are presented as raw X-ray counts without matrix corrections. Reaction rim widths were measured from between 5 and 10 BSE

**Table 1**  
Temperature and duration of reaction, thicknesses of reaction layers and intergrowths, and area-ratios of layers and intergrowth regions in MgO–garnet reaction experiments at 20 GPa.

Run #	T (K)	t (s)	X <sub>1</sub> (μm)	X <sub>2</sub> (μm)	A <sub>2</sub> /A <sub>1</sub>
H2743	1773	14 400	1.5 (3) <sup>a</sup>	12 (3)	1.00 (8)
H3252	1773	50 400	3.0 (6)	23 (2)	1.7 (4)
H3251	1773	154 800	4.6 (7)	26 (3)	1.14 (9)
H2697	1873	3600	2.6 (2)	13 (2)	1.0 (2)
H2696	1873	14 400	3.2 (5)	17 (3)	1.3 (1)
H2744	1873	37 800	4.0 (4)	22 (2)	1.0 (3)
H2581	1873	108 000	9 (1)	30 (4)	1.0 (1)
H2742	1973	3600	4.2 (9)	14.6 (2)	1.06 (09)
H2585	2123 (50)	1800	19 (4)	59 (5)	0.8 (2)
H2587	2123 (50)	7200	23 (3)	49 (17)	0.29 (7)
H2583	2123 (50)	36 000	33 (2)	94 (12)	0.5 (1)
MA1k/1345	1923	7200	10.2 (8) <sup>b</sup>	–	1.2 (2) <sup>c</sup>

<sup>a</sup> Means of 5 to 10 measurements with 1 standard error values in parentheses (in the last digit of the mean).

<sup>b</sup> In this Al-free experiment the layer and intergrowth regions produce a single layer (see text for details).

<sup>c</sup> The boundary between layer 1 and layer 2 is defined by the presence/absence of CaSiO<sub>3</sub> grains.

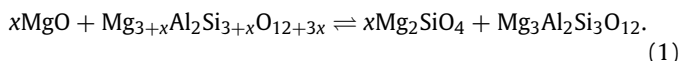
images. These agreed within error with rim widths determined from the compositional line-profiles. Areas of reaction zones were determined by manually drawing around the ringwoodite layer and the areas of these drawings were determined using the ImageJ programme (Schneider et al., 2012). In the rare cases where the backscattering contrast between the different phases was sufficiently strong to determine phases by automatic thresholding the image, the measured areas agreed with areas determined by drawing. In order to investigate any possible topotaxy several samples were first chemically polished to high quality, using 0.03 μm colloidal silica in an alkaline solution, then coated with a <5 nm layer of carbon and analysed by electron back-scattered diffraction (EBSD) in the X500 CrystalProbe field emission gun (FEG) SEM at the University of Liverpool. Electron back-scatter diffraction patterns (EBSPs) were obtained using 20 kV accelerating voltage, 35 nA beam current and 25 mm working distance. EBSPs were automatically indexed using the software package CHANNEL 5, and crystallographic misorientations were calculated between neighbouring data points with 0.25 μm grid spacing. Errors in the measurement of orientations are within ±0.5°. All EBSD analyses were carried out with simultaneous element mapping, using energy dispersive spectroscopy (EDS), so that measured crystallographic orientations could be associated unequivocally with each of the phases present. Chemically polished samples were also imaged in forward-scattering geometry to produce orientation contrast images using the Leo 1530 FEG SEM installed at the Bayerisches Geoinstitut.

### 3. Results

Fig. 1 shows scanning electron microscope images of the reaction region from experiment H2744 (1873 K, 10.5 h; Fig. 1A, B), along with a compositional profile across the interface on the iron-bearing side of the sample. There is a strong Z-contrast between the different phases, with MgO appearing dark, Mg<sub>2</sub>SiO<sub>4</sub> (ringwoodite) intermediate and (Mg,Al)(Al,Si)O<sub>3</sub> (garnet) light grey; iron-bearing samples (Fig. 1B) are lighter than iron-free samples (Fig. 1A). The assignment of the different regions to MgO, ringwoodite and garnet is confirmed by the compositional profile (Fig. 1E), with (Mg + Fe)/Si ratios of 1 and 2 respectively for the light and intermediate regions. The interface between the MgO and ringwoodite is sharp and planar, whereas ringwoodite and garnet form a complex intergrowth at their mutual interface. This intergrowth is seen in all the experiments containing alumina in the starting garnet composition.

#### 3.1. Interface growth and instability mechanism

Milke et al. (2009) observed a complex interface between enstatite and quartz in quartz–olivine reaction experiments in a system where stress in the quartz matrix controlled the interface growth kinetics (see also Schmid et al., 2009). While reduction of interface stress is a plausible mechanism for developing interfacial instabilities it is not the only mechanism. We suggest that the complex intergrowth observed here results from a double-diffusive instability. Fig. 1E shows a compositional profile across the reaction zone shown in Fig. 1B. The aluminium content of the ringwoodite in both the layer and the intergrowth region is below the detection limit, with aluminium contents in the garnet immediately adjacent to the ringwoodite layer of 10%, 2.5 times higher than the initial aluminium content. As ringwoodite grows it consumes a majoritic (MgSiO<sub>3</sub>) component, expelling a residual pyrope (Mg<sub>3</sub>Al<sub>2</sub>Si<sub>3</sub>O<sub>12</sub>) component into the remaining garnet:



An increased pyrope content in the garnet reduces the chemical potential of majorite in the garnet, thereby inhibiting further reaction. Interdiffusion between majorite and pyrope garnets is extremely slow (van Mierlo et al., 2013) resulting in a reaction at the interface between garnet and ringwoodite which is rate limited by aluminium diffusion away from the growing interface. In addition to interdiffusion within the garnet, the pyrope concentration at the growing ringwoodite interface can be reduced by increasing the area of the interface at which pyrope is expelled, resulting in a complex symplectite texture in the reaction rim. We tested this model by performing one experiment in an alumina-free system which should have a planar reaction rim if the instability is double-diffusive but which should still have a complex interface if it is due to matrix stresses (Fig. 1C). The interface between garnet and ringwoodite is a simple planar feature in this experiment, confirming that the symplectite texture observed here in Al-bearing experiments is due to a double-diffusive instability. The experiments performed here differ from those of Milke et al. (2009) in one important respect: here we used parallel sided plates of MgO whereas Milke et al. used spherical grains in a reactive matrix. The analysis of Schmid et al. (2009) implies that matrix stress will dominate for small grains and diffusion will dominate for large grains. The surfaces of the MgO discs used in the experiments presented here may be described as having a very large radius of curvature, equating to large effective grain sizes. This supports the inference that complex intergrowth at the ringwoodite–majorite interface results from diffusive processes.



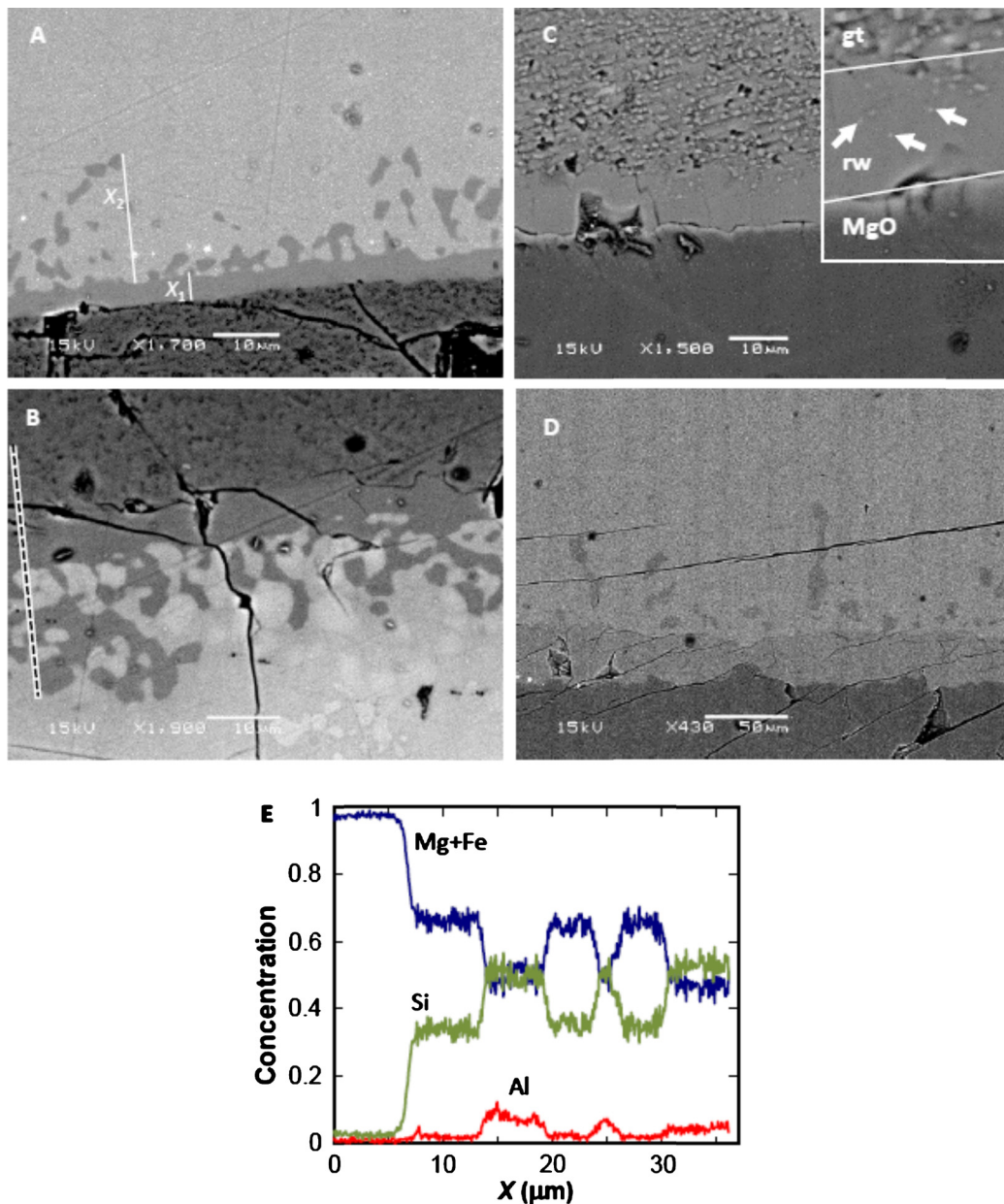


**Fig. 1.** Scanning electron micrographs of reaction zones between MgO and garnet. (A) Al-bearing reacted at 1873 K for 37 800 s; (B) Al- and Fe-bearing reacted at 1873 K for 37 800 s; (C) Al-free reacted at 1923 K for 7200 s. Arrows in the enlarged inset mark the  $\text{CaSiO}_3$  perovskite grains which indicate the position of the original MgO–garnet interface; (D) Al-bearing reacted at 2123 K for 36 000 s. (E) Measured concentration profiles along the line marked in (B).

It is interesting to note that, at the highest temperatures investigated in our experiments, the intergrowth is less well developed, appearing as an undulating interface between garnet and ringwoodite, with occasional fingers of ringwoodite extending from the reaction rim (Fig. 1D). This could be due either to an increased solubility of aluminium in ringwoodite or to an increased interdiffusion coefficient in the garnet relative to the ringwoodite growth rate. Ab initio simulations studies of cation disordering in ringwoodite (Panero, 2008) suggest that, in the  $P$ – $T$  range of the current experiments, there could be up to 4% anti-site occupancy (Si on Mg sites and Mg on Si sites) with the anti-site concentration varying by  $\sim 1\%$  per 100 K. This might also suggest that aluminium becomes increasingly soluble in ringwoodite at high temperature since aluminium cations have a volume and valency which is intermediate between magnesium and silicon. The mean aluminium content of ringwoodite at 2123 K was found to be  $0.3 \pm 0.06$  wt%, compared with no detectable aluminium at lower temperatures.

This *might* suggest that increased aluminium solubility in ringwoodite inhibits the development of the intergrowth region, however the aluminium concentration gradient in garnet in the high- $T$  experiments is similar to that at lower temperatures.

### 3.2. Ringwoodite growth kinetics

In the case of diffusion controlled kinetics, the rate of growth of the interface is linear with the square-root of time (see Watson and Price (2002) for discussion of spinel growth in the  $\text{MgO}$ – $\text{Al}_2\text{O}_3$  system). In determining the kinetics of reaction involving growth of interface products it is therefore customary to present graphs of width of the reaction zone as a function of time. However, for the complex interface encountered in the present experiments, such a representation is problematic: how is the reaction-zone width defined? We chose to present two distinct parameters (Fig. 1A) defined as follows: (1) The minimum distance between MgO and

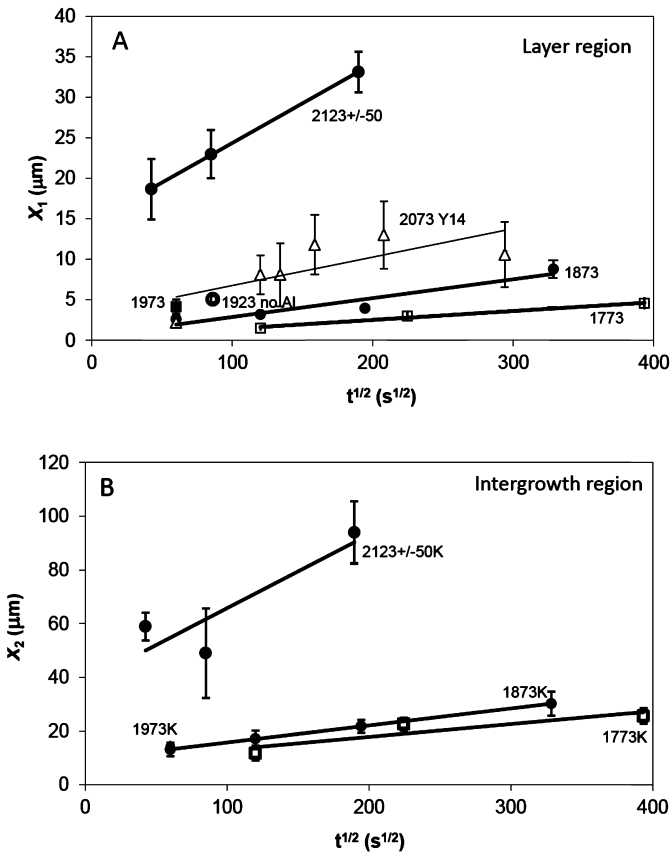


**Fig. 2.** Measured reaction zone thicknesses plotted against time squared: (A) Layer thickness, (B) intergrowth thickness. Both thickness measurements are linear with time squared, consistent with reaction controlled by bulk diffusion. The triangles, labelled Y14, are from Shimojuku et al. (2014), for  $\text{MgSiO}_3$  perovskite– $\text{MgO}$  reaction at 22.5 GPa.

garnet is measured in a series of images of the same interface in a given recovered sample. The width of this pure-ringwoodite layer ( $X_1$ ) is quoted as the mean of these measurements (Fig. 2A). (2) We also define a width of the ringwoodite–garnet intergrowth region ( $X_2$ ) as the maximum extent of the ringwoodite away from the  $\text{MgO}$ , measured perpendicular to the  $\text{MgO}$  interface, minus  $X_1$  (Fig. 2B). As before, the mean intergrowth width for each experiment is obtained by averaging several measurements. Throughout the paper we use the subscripts 1 and 2 to refer to the ringwoodite layer and intergrowth region respectively. The widths of the ringwoodite layer and the intergrowth region are presented in Table 1 and Fig. 2 and both show a linear dependence on the square-root of time, consistent with diffusion controlled growth. At the highest temperature, reaction during the approach to the final experimental temperature is significant, resulting in positive values of  $X_1$  and  $X_2$  at zero time, however subsequent growth is linear with  $t^{1/2}$ . Converting these interface thickness measurements at each temperature into apparent rate constants, following the treatment of Tammann (1920):

$$k = \frac{dX^2}{2dt} \quad (2)$$

yields Arrhenius curves for growth of the ringwoodite, and ringwoodite–garnet intergrowth layers, as shown in Fig. 3. The pre-exponential factors and activation enthalpies for growth are  $\ln(k_1^0) = -6.36 \pm 0.25 \text{ m}^2/\text{s}$  and  $E_1 = 456 \pm 40 \text{ kJ/mol}$  for the ringwoodite layer, and  $\ln(k_2^0) = -9.2 \pm 3.3 \text{ m}^2/\text{s}$  and  $E_2 = 371 \pm 53 \text{ kJ/mol}$  for the intergrowth region. These activation enthalpies agree, within error, with the activation enthalpies of Si-diffusion

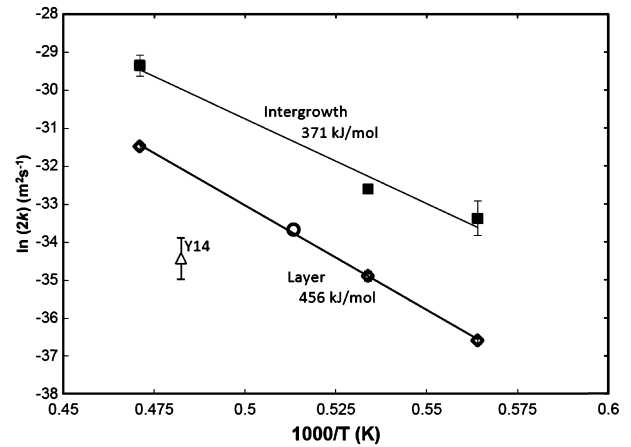


**Fig. 3.** Arrhenius plot of apparent rate constant,  $k$ , for the ringwoodite layer and intergrowth regions. The circle is derived from the apparent reaction rate constants for Al-bearing samples at 1973 K and Al-free samples at 1923 K; this datum is not used for deriving the Arrhenius fit for the layer growth as it has a considerable error associated with the varying temperature and aluminium contents of the two experiments. However, it is consistent with the other experiments suggesting that the kinetics of the growth of the ringwoodite layer is the same regardless of the aluminium content of the garnet. The triangle, labelled Y14, is from the data of Shimojuku et al. (2014), for  $\text{MgSiO}_3$  perovskite– $\text{MgO}$  reaction at 22.5 GPa.

in ringwoodite ( $E_{\text{lat}} = 483 \pm 94 \text{ kJ/mol}$ ,  $E_{\text{gb}} = 402 \pm 88 \text{ kJ/mol}$ ; Shimojuku et al., 2009) and pyrope–majorite interdiffusion ( $E = 291 \pm 51 \text{ kJ/mol}$ ; van Mierlo et al., 2013;  $E = 369 \pm 47 \text{ kJ/mol}$ ; Nishi et al., 2013). It should be noted that, since the intergrowth region contains a mixture of reaction product (ringwoodite) and unreacted garnet,  $k_2$  cannot be used to calculate a reaction rate, but rather describes the width of the intergrowth region. On the other hand, if the layer of ringwoodite reflects the consumption of  $\text{MgO}$ , as we argue below,  $k_1$  is a true rate constant and can be used to calculate rate of consumption of  $\text{MgO}$  in this system.

The growth of ringwoodite at the interface between  $\text{MgO}$  and garnet, according to the simplified reaction:



is kinetically inhibited in the experimental arrangement (and in the Earth) by a layer of product material forming between the reactants. For the reaction to proceed reactant material must be transported across the growing ringwoodite layer;  $\text{MgO}$  can diffuse towards the garnet interface or  $\text{SiO}_2$  can diffuse towards the  $\text{MgO}$  interface as cartooned in Fig. 4, or a mixture of both can occur. In the case of magnesium diffusion (Fig. 4a), ringwoodite grows at the garnet interface according to reaction (3) and  $\text{MgO}$  dissolves into the ringwoodite at the  $\text{MgO}$  interface. Thus, while the  $\text{MgO}$  crystal is consumed by the reaction, ringwoodite does not grow at the point of  $\text{MgO}$  dissolution to fill the void left by the diffusing  $\text{MgO}$  volume. Rather, the ringwoodite is produced at the interface with garnet, with a resultant local volume increase, and the entire ringwoodite layer must then relax in response to the stress gradient produced by dissolving  $\text{MgO}$  at one interface and growing ringwoodite at the other.

In the case of silicon diffusion (Fig. 4b), however, ringwoodite is produced in equimolar ratios at both interfaces through the two half reactions, at the ringwoodite–garnet interface:



and, at the  $\text{MgO}$ –ringwoodite interface:



In this case, the volume of the growing ringwoodite at both interfaces is more nearly balanced by the volume of the consumed reactants, requiring much less relaxation of the ringwoodite layer.

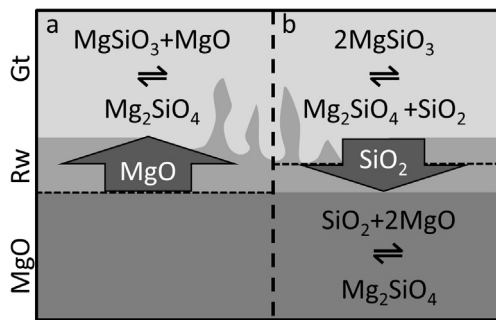


**Fig. 4.** Cartoon of ringwoodite growth under different limiting diffusion mechanisms: (a) Diffusion of MgO through the layer results in growth of ringwoodite at the garnet interface only. (b) Diffusion of  $\text{SiO}_2$  through the layer results in ringwoodite growth at both garnet and MgO interfaces. A marker at the original MgO-garnet interface would remain in contact with MgO in the case of magnesium diffusion but would be included within the reaction zone in the case of silicon diffusion. Aluminous bulk compositions result in a complex intergrowth geometry at the ringwoodite-garnet interface (central region of the cartoon), whereas Al-free compositions have straight interfaces on both sides of the ringwoodite.

The continued growth with time of both the ringwoodite layer ( $X_1$ ) and the intergrowth region ( $X_2$ ) suggests that ringwoodite is produced at both the interfaces in contact with MgO and garnet, rather than just at the interface in contact with garnet (which would favour growth of  $X_2$ ).

This is confirmed by the mass-balance between the ringwoodite in the layer and the intergrowth regions. The ratio of the area of the ringwoodite in the intergrowth ( $A_2$ ) and the area of the ringwoodite in the layer ( $A_1$ ) as measured from SEM images is unity, within error, for all experiments except those at the highest temperature (Table 1). This suggests that measured cross-sectional areas can be used as proxies for the volumes of ringwoodite in the layer and the intergrowth region since the cross-sections prepared from recovered samples were randomly oriented sections cut perpendicular to the MgO plate. Thus the volumes of ringwoodite are equal in the two regions in experiments up to 1973 K. This is consistent with diffusion of  $\text{SiO}_2$  controlling the reaction and the original interface between MgO and garnet being located at the transition between the ringwoodite layer and the intergrowth region at lower temperatures. This is further supported by the Al-free experiment where the garnet starting glass contained a small amount of  $\text{CaSiO}_3$ . This produces calcium-silicate perovskite at the pressure of the experiments which does not participate in the reaction and acts as an inert marker of the original interface. In this experiment, the  $\text{CaSiO}_3$  impurity grains are contained within the half of the ringwoodite layer in contact with garnet, but not in the half of the layer in contact with MgO (Fig. 1C) implying that in this experiment the original interface was located at the centre of the growing ringwoodite layer. Furthermore, if the thickness of the ringwoodite layer produced in the Al-free experiment is halved it agrees well with the growth rate of the ringwoodite layers in the Al-bearing experiments (Figs. 2 and 3) i.e., the total growth rate of ringwoodite in the Al-free experiment is twice the growth rate of the ringwoodite layers in the Al-bearing experiments. This is consistent with diffusion of  $\text{SiO}_2$  controlling the growth of ringwoodite in this system. It is surprising that silicon diffusion controls growth of the ringwoodite when magnesium diffusion is much faster than silicon diffusion in ringwoodite (e.g. Farber et al., 2000), however the activation enthalpy of the rate constant and the mass balance at either side of the growing ringwoodite both argue strongly for silicon diffusion. Possibly grain-boundary diffusion of silicon is faster than lattice diffusion of magnesium at the small grain sizes of the ringwoodite in the present experiments, but this hypothesis cannot be tested until magnesium diffusion coefficients are measured for ringwoodite. A final possibility is that the slowest

diffusing species is oxygen, in which case both Mg-diffusion and Si-diffusion will be active in the growing ringwoodite layer. Due to the difficulty of accurately measuring the volume of ringwoodite in the intergrowth layer it is not possible here to unequivocally determine the dominant mass transport mechanism. However, all of the observations are consistent with Si-diffusion being the controlling process.

### 3.3. Growth fabric

Results from an electron-backscattered diffraction study of experiment H2742 (1973 K, 1 h) are presented in Fig. 5. The MgO plate was broken into several large pieces during this experiment, resulting in 4 large MgO domains at the bottom of Fig. 5a (note that grains can be visualised as domains of distinct colour in all phases). Ringwoodite in the layer next to MgO forms grains of up to 5  $\mu\text{m}$  diameter (Fig. 5b) and tends to have phase boundaries with MgO in which ringwoodite (001) planes are closer to MgO (001) orientations than a random distribution (Fig. 5c), however the texture is not strong. The mean grain size in the intergrowth region (Fig. 5d) is much smaller, at  $1.6 \pm 0.1 \mu\text{m}$  and ringwoodite-garnet phase boundaries are closer to random than the ringwoodite-MgO phase boundaries. Grain growth appears to be very slow in the intergrowth region, not changing significantly between experiments with different amounts of reaction, as seen from the orientation contrast map of the reaction region in experiment H2581 (1873 K, 30 h), Fig. 6. The grain size of garnet away from the intergrowth region is larger than either the layer or intergrowth regions.

## 4. Discussion

### 4.1. Comparison with previous results

Only one previous study has investigated the retrograde reaction across the 660 km discontinuity: Shimojuku et al. (2014) reacted  $\text{MgSiO}_3$  perovskite single crystals with MgO single crystals at 22.5 GPa and 1800 °C. Rim thicknesses and the derived reaction rate constant from Shimojuku et al. (2014) are plotted in Figs. 2A and 3: they are comparable to, but somewhat slower than, those of the present study. The apparent activation volume for the reaction rate constant can be calculated by combining the present data with those of Yoshino et al. on the assumption that the two studies are directly comparable. This yields a value of 17  $\text{cm}^3/\text{mol}$ , which is unreasonably large for defect migration in silicates and suggests that some factor other than pressure is causing the reduced reaction rate in the previous study compared to this one. One possibility is that the presence of perovskite rather than garnet on the silica-rich side of the reaction couple reduces reaction rates by changing either the stress-field or the activities of the diffusing species in the ringwoodite layer. A more likely explanation might be that the excess free energy of reaction is higher in the present, low-pressure, experiments resulting in a larger driving force for the reaction. Shimojuku concluded, on the basis of Pt-markers which remained at the MgO interface during reaction, that the diffusing component was MgO. However Watson and Price (2002) found that Pt was prone to adhere preferentially to MgO resulting in a false attribution of Mg-diffusion as the mass transport process. For this reason we chose not to use Pt as the passive marker but, rather a system which produced  $\text{CaSiO}_3$  perovskite grains to act as passive markers. In this case, the presence of  $\text{CaSiO}_3$  grains in the portion of the ringwoodite film closest to the garnet suggested that Si-diffusion contributed to the growth kinetics. It is possible that the controlling species is different for garnet-MgO and perovskite-MgO reaction, although this seems unlikely. The diffusing species controlling ringwoodite layer growth is thus still open to debate,



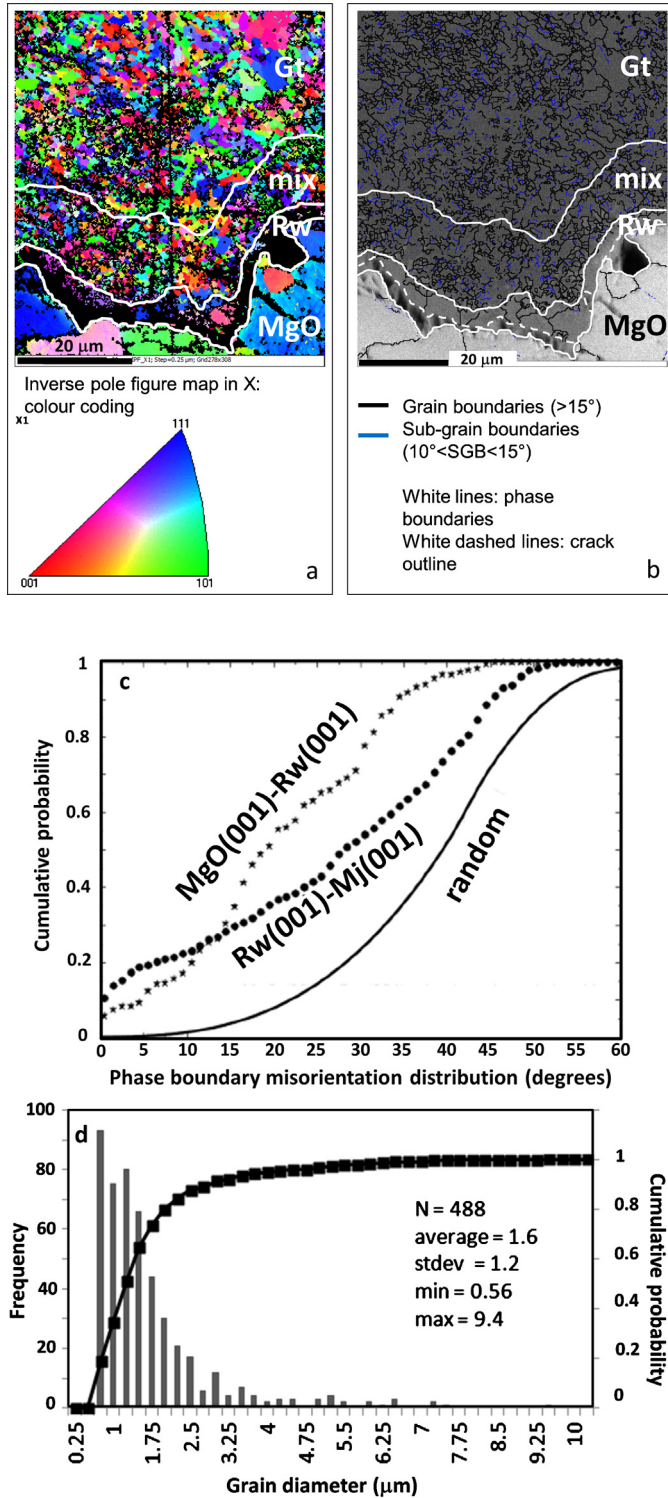


**Fig. 5.** (a) Inverse pole figure map from electron backscatter diffraction (EBSD) measurements of the periclasite-majorite interface region in experiment H2742 (1973 K, 3600 s). The map shows grain orientations relative to the X direction (horizontal) and it is colour-coded for crystallographic directions (see legend). Black areas indicate non-indexed zones. (b) Grain boundary map of the same area from EBSD measurements. Grain boundaries (>15° misorientation) are shown in black and sub-grain boundaries (<15°) in blue. In all images white lines delimit phase and mixed phase boundaries. (c) Fabric relationships of phase boundaries between MgO and ringwoodite, and ringwoodite and majorite for (001)(001). The indexing of the garnet assumes that it is cubic, which is reasonable given the aluminium content of garnet in the intergrowth region (see, for example, Hunt et al., 2010). (d) Grain size distribution for the intergrowth region. Grain sizes in the mixed ringwoodite-majorite interlayer are all <10 μm and average <2 μm.

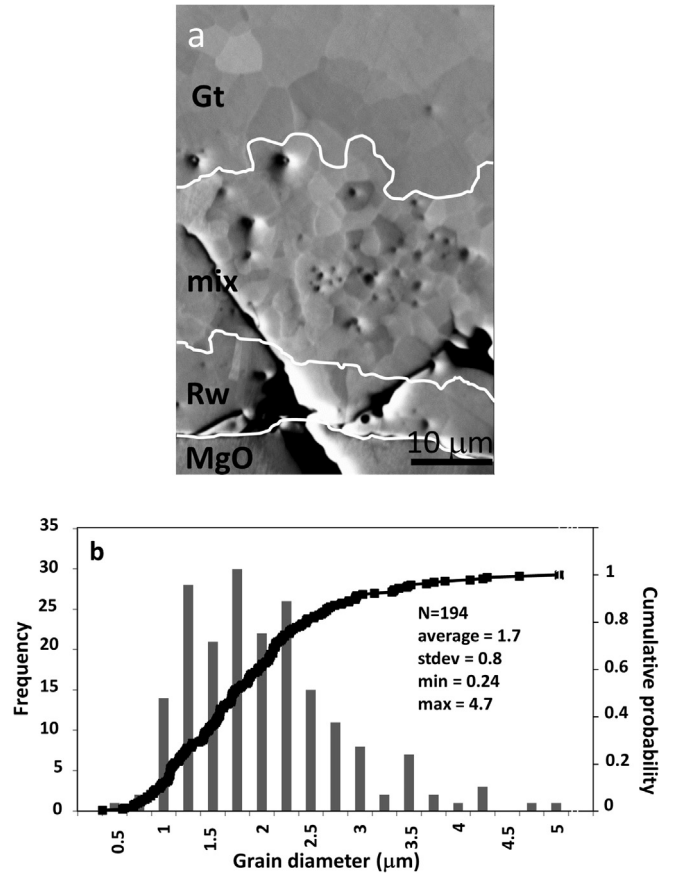


**Fig. 6.** (a) Orientation contrast image (OCI) of experiment H2581 (1873 K, 108 000 s) which shows the grain structure in the interface region. (b) Grain size distribution for the intergrowth region. The grain size distribution is very similar to that in Fig. 5d despite a factor two difference between the thickness of the intergrowth in the two experiments.

however this does not affect the following discussion regarding the kinetics of reaction and implications for the mantle.

#### 4.2. The kinetics of the retrograde reaction above the 660 km discontinuity

We now use the reaction rate for production of the ringwoodite layer to calculate the time that ferropericlasite grains would persist metastably in regions upwelling through the 660 km discontinuity. Given the mass-balance between the ringwoodite in the layer and intergrowth regions we can estimate the total volume of ringwoodite produced as twice the volume of the layer region. The volume of ferropericlasite consumed is therefore related to the volume of ringwoodite in the layer according to the volumes of reaction:

$$-V_{\text{Fp}}/V_1 = 2\bar{V}_{\text{Fp}}/\bar{V}_{\text{Rw}} = 0.57, \quad (5)$$

where the  $-V_{\text{Fp}}$  and  $V_1$  are the volumes of ferropericlasite consumed and ringwoodite produced in the layer and  $\bar{V}_{\text{Fp}}$ ,  $\bar{V}_{\text{Rw}}$  are the molar volumes of ferropericlasite and ringwoodite. The rate of consumption of ferropericlasite in upwelling regions of mantle at 660 km depth depends on the geometry of the ferropericlasite. Here we consider two end-members: (i) a semi-infinite layer of ferropericlasite bounded on both sides by garnet, corresponding to a mineralogically layered texture in the uppermost lower mantle, and (ii) a spherical grain of ferropericlasite embedded in garnet, corresponding to randomly distributed MgO and perovskite in the lower mantle. In both cases we assume that the garnet and periclasite are weak media of infinite extent and ignore nucleation kinetics allowing us to consider only the diffusion problem.

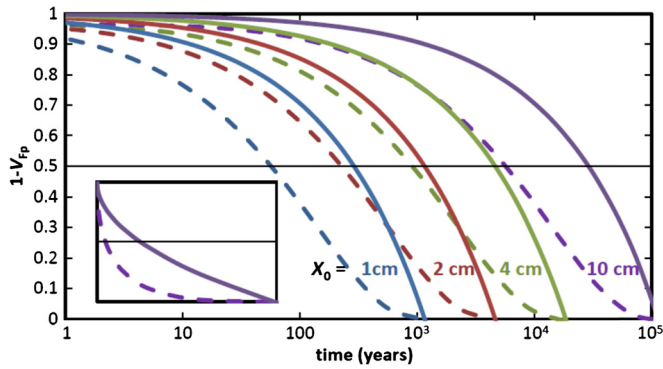


**Fig. 7.** Consumption as a function of time for ferropericlasite grains (dotted lines) and layers (solid lines) of different initial sizes in a pyrolytic mantle assemblage ascending through the 660 km discontinuity.  $X_0$  is the initial radius (or half the layer thickness). The inset plot is for reaction of grains and layers with only one value of  $X_0$  plotted against linear time to show the strong non-linearity of reaction rate of grains.

In the first case the rate of consumption of ferropericlasite at each interface is, from (2) and (5):

$$dX = 0.57 \times \sqrt{2k_1 dt}. \quad (6)$$

In the second case, the rate of consumption of spherical grains is given by Schmid et al. (2009):

$$\frac{dV_{Fp}}{dt} = -k_1 \frac{r_{Fp} r_1}{r_{Fp} - r_1} \times \frac{4\pi r_{Fp}^2}{X_0^2}, \quad (7)$$

where the reaction rate constant,  $k_1$ , includes the terms for the effective combined diffusivity of magnesium and silicon across the interface, the Gibbs free energy and the molar volume of ferropericlasite in Eq. (10) of Schmid et al. (2009). The variables  $r_{Fp}$  and  $r_1$  are the radii of the inner and outer edges of the ringwoodite layer at time,  $t$ , and  $V_0$  and  $X_0$  are the volume and radius of the ferropericlasite grain at  $t = 0$ . The radius at the outer edge of the ringwoodite layer is, from mass balance:

$$r_1 = \left( \frac{3(V_{Fp} + \{V_0 - V_{Fp}\}/0.57)}{4\pi} \right)^{1/3}. \quad (8)$$

Ferropericlasite consumption for the two cases is presented as a function of time in Fig. 7 for reaction at 1873 K. The reaction rate of spheres is significantly more non-linear in time than the reaction rate of sheets, with spheres initially reacting much faster than sheets; 50% reaction is seven times faster for spheres than for sheets with the same initial size, but 95% reaction is only twice as fast for spheres. Seismic observations would therefore more readily observe the thickness of a layered texture around the 660 km discontinuity, where the effective reaction width is wider than in spheres of an equivalent size, than an isotropic texture: the effect of grain size on the width of the 660 km seismic discontinuity will be addressed in a separate paper.

#### 4.3. Implications for the mantle above 660 km

The complex ringwoodite–garnet intergrowth texture observed in Al-bearing samples has implications for the grain size and (potentially) strength of the deep transition zone. The reaction produces an inherited texture from the lower-mantle assemblage with ringwoodite replacing the original ferropericlasite grains and garnet replacing perovskite. At the interface between ringwoodite and garnet there is a fine-grained intergrowth zone which, in the present experiments, contains one half of the ringwoodite and is approximately 25 vol% ringwoodite, 75 vol% garnet. Ringwoodite

comprises approximately 60 vol% of the deep transition zone suggesting that, if the mass balance observed here pertains to the retrograde reaction at 660 km depth in the Earth, all of the garnet will become included in the reaction intergrowth and this intergrowth will occupy 70 vol% (with 30% ringwoodite and 40% garnet) once the reaction is complete. The reaction zone is likely to be less than 1 km thick for reasonable lower-mantle grainsizes (Fig. 7) and upwelling rates but regions consisting of the ringwoodite–garnet intergrowth will not readily coarsen due to Zener pinning (e.g. Hillert, 1965). This will result in a region at the base of the transition zone which consists of ringwoodite grains (of similar size to the ferropericlasite grains from which they were derived) embedded in a fine-grained mixture of ringwoodite and garnet. The present experiments suggest that the grain size of perovskite is reset to a small value during mantle upwelling through the 660 km discontinuity, however the grain size of ferropericlasite might persist as a palimpsest texture of ringwoodite porphyroblasts within a fine-grained ringwoodite–garnet matrix. It might be possible for this texture to be preserved during ascent through the upper mantle, since the  $(\text{Mg,Fe})_2\text{SiO}_4$  porphyroblasts will have a larger grain size, and will coarsen more quickly, than the mixed-phase matrix. This will result in the porphyroblasts being stronger than the matrix and, hence, they might survive shear deformation during mantle upwelling and exhumation. Such palimpsest textures might be detected by variations in the trace-element chemistry between porphyroblastic- and matrix-olivine in appropriate xenoliths since the former would have originated from ferropericlasite and the latter from perovskite.

The present experiments also have implications for the rheology of the transition zone. The observed grain size of the intergrowth ( $\sim 2 \mu\text{m}$ ) is sufficiently small for diffusion creep to dominate, implying that the transition zone above 660 km in regions of mantle upwelling should be weaker than either the lower mantle or the overlying transition zone. This region might be further weakened by reaction-mediated diffusion creep, which is not rate-limited by the slowest diffusing species (Wheeler, 1992; Bruhn et al., 1999; Sundberg and Cooper, 2008). We speculate that weakening associated with mantle upwelling through 660 km depth might result in a degree of viscous decoupling between the upper and lower mantle as suggested from some inversions of the geoid, postglacial rebound and seismic tomography data (e.g. Mitrova and Forte, 2004). We emphasise here that the region of fine-grained intergrowth would have considerable lateral variability in its thickness, ranging from zero in regions of downwelling and being a maximum for rapidly upwelling regions of large lower-mantle grain size. This is consistent with the analysis of Paulson and Richards (2009) who concluded that geophysical studies of radial viscosity structure in the mantle ‘are compatible with the existence, in at least some if not most geographical settings’ with a narrow region within the upper mantle with a very low viscosity. The low-viscosity region atop 660 km invoked here might be most significant for upwelling plumes which have upwelling rates of several tens of centimetre per year (e.g. Farnetani and Hofmann, 2009) and which might be coarser than the surrounding mantle (e.g. Solomatov, 1996; Korenaga, 2005). The increased plume temperature of, perhaps 500 K hotter than the normal mantle, will act against these factors increasing reaction rates by one order of magnitude: this effect is small compared to the effect of the enhanced upwelling rate at plumes.

Without further experimental studies it is difficult to estimate the thickness and strength reduction of such a layer. However, if we assume that diffusion creep dominates for grain sizes of  $10 \mu\text{m}$  or less, using the grain-growth kinetics for pure ringwoodite (Yamazaki et al., 2005) the region with reduced strength would be approximately 1 km thick for mantle upwelling at a rate of 10 cm/yr. This is likely to be a substantial



underestimate of the thickness of the weak layer since it takes no account of the effect of Zener pinning on reducing grain-growth rates. Layers in the upper mantle with reduced viscosity tend to reduce the diameter and increase the velocity of the upwelling plume in the low-viscosity region. While there have been no studies of the effect of a very low viscosity layer of a few kilometres thickness, Leng and Gurnis (2012) found that low-viscosity layers placed within the upper mantle and transition zone tended to reduce the size of plumes reaching the Earth's surface, with larger effects for thinner layers.

Here we have considered relatively simple compositions in the Mg–Al–Si–O and Fe–Mg–Al–Si–O systems but it appears that the main effect on the reaction comes from the presence or absence of Al. Our compositions with 3–5%  $\text{Al}_2\text{O}_3$  encompass the alumina contents of pyrolite and MORB-source mantle and there was no difference observed in the behaviours of the different compositions. We are therefore confident that the present results are applicable to both normal mantle and any enriched mantle component involved in deep-mantle plume-like upwellings. In order to quantify the extent of the viscosity reduction in upwellings above 660 km depth further work is required to determine both the degree of weakening and the grain-growth rate in ringwoodite garnet mixtures produced by the retrograde reaction of perovskite plus ferropericlase to ringwoodite.

## Acknowledgements

We wish to thank C. Liebske, J. Badro and I.G. Wood for helpful discussions. The high-pressure experiments were largely performed at the Bayerisches Geoinstitut under the aegis of an EU large-scale facility grant to D. Rubie and an Alexander von Humboldt fellowship to D. Dobson. The Al-free experiment was performed at the ETH Zurich during a visiting professorship by D. Dobson. We acknowledge funding from NERC (grants NE/L006898 and NE/L007363). The manuscript was improved by the helpful reviews of T. Kubo and two anonymous reviewers.

## References

- Akaogi, M., Tanaki, A., Ito, E., 2002. Garnet-ilmenite-perovskite transitions in the system  $\text{Mg}_4\text{Si}_4\text{O}_{12}$ – $\text{Mg}_3\text{Al}_2\text{Si}_3\text{O}_{12}$  at high pressures and high temperatures: phase equilibria, calorimetry and implications for mantle structure. *Phys. Earth Planet. Inter.* 132, 303–324.
- Bruhn, D.H., Olgaard, D.L., Dell'Angelo, L.N., 1999. Evidence for enhanced deformation in two-phase rocks: experiments on the rheology of calcite-anhydrite aggregates. *J. Geophys. Res.* 104, 707–724. <http://dx.doi.org/10.1029/98JB02847>.
- Dobson, D.P., Vočadlo, L., Wood, I.G., 2002. A new high-pressure phase of FeSi. *Am. Mineral.* 87, 784–787.
- Farber, D.L., Williams, Q., Ryerson, F.J., 2000. Divalent cation diffusion in  $\text{Mg}_2\text{SiO}_4$  spinel (ringwoodite),  $\beta$  phase (wadsleyite), and olivine: implications for the electrical conductivity of the mantle. *J. Geophys. Res.* 105, 513–529.
- Farnetani, C.G., Hofmann, A.W., 2009. Dynamics and internal structure of a lower mantle plume conduit. *Earth Planet. Sci. Lett.* 282, 314–332.
- Hillert, M., 1965. On the theory of normal and abnormal grain growth. *Acta Metall.* 13, 227–238.
- Hiraga, T., Tomonori, M., Miki, T., Hidehiro, Y., 2010. Mantle superplasticity and its self-made demise. *Nature* 468, 1091–1095. <http://dx.doi.org/10.1038/nature09685>.
- Hirose, K., 2002. Phase transitions in pyrolitic mantle around 670-km depth: implications for upwelling of plumes from the lower mantle. *J. Geophys. Res.* 107, 2078. <http://dx.doi.org/10.1029/2001JB000597>.
- Hunt, S.A., Dobson, D.P., Weidner, D.J., Li, L., Brodholt, J.P., Walte, N.P., 2010. Relative strength of the pyrope-majorite solid solution and the flow-law of majorite-containing garnets. *Phys. Earth Planet. Inter.*, 87–95. <http://dx.doi.org/10.1016/j.pepi.2009.12.001>.
- Ito, E., Takahashi, E., 1989. Postspinel transformations in the system  $\text{Mg}_2\text{SiO}_4$ – $\text{Fe}_2\text{SiO}_4$  and some geophysical implications. *J. Geophys. Res.* 94, 10637–10646.
- Korenaga, J., 2005. Firm mantle plumes and the nature of the core–mantle boundary region. *Earth Planet. Sci. Lett.* 232, 29–37.
- Kubo, T., Ohtani, E., Kato, T., Urakawa, S., Suzuki, A., Kanbe, S., Funakoshi, K.-I., Utsumi, W., Kikegawa, T., Fujino, K., 2000. Formation of metastable assemblages and mechanisms of the grain-size reduction in the postspinel transformation of  $\text{Mg}_2\text{SiO}_4$ . *Geophys. Res. Lett.* 27 (6), 807–810. <http://dx.doi.org/10.1029/1999GL008430>.
- Kubo, T., Ohtani, E., Kato, T., Urakawa, S., Suzuki, A., Kanbe, S., Funakoshi, K.-I., Utsumi, W., Kikegawa, T., Fujino, K., 2002. Mechanisms and kinetics of the post-spinel transformation in  $\text{Mg}_2\text{SiO}_4$ . *Phys. Earth Planet. Inter.* 129, 153–171. [http://dx.doi.org/10.1016/S0031-9201\(01\)00270-9](http://dx.doi.org/10.1016/S0031-9201(01)00270-9).
- Leng, W., Gurnis, M., 2012. Shape of thermal plumes in a compressible mantle with depth-dependent viscosity. *Geophys. Res. Lett.* 39, L05310. <http://dx.doi.org/10.1029/2012GL050959>.
- van Mierlo, W.L., Langenhorst, F., Frost, D.J., Rubie, D.C., 2013. Stagnation of subducting slabs in the transition zone due to slow diffusion in majoritic garnet. *Nat. Geosci.* 6, 400–403. <http://dx.doi.org/10.1038/NNGEO1772>.
- Milke, R., Abart, R., Kunze, K., Koch-Müller, M., Schmid, D., Ulmer, P., 2009. Matrix rheology effects on reaction rim growth I: evidence from orthopyroxene rim growth experiments. *J. Metamorph. Geol.* 27 (1), 71–82.
- Mitrovica, J.X., Forte, A.M., 2004. A new inference of mantle viscosity based upon joint inversion of convection and glacial isostatic adjustment data. *Earth Planet. Sci. Lett.* 225, 177–189.
- Nishi, M., Kubo, T., Ohfuji, H., Kato, T., Nishihara, Y., Irifune, T., 2013. Slow Si–Al interdiffusion in garnet and stagnation of subducting slabs. *Earth Planet. Sci. Lett.* 361, 44–49.
- Nishiyama, N., Irifune, T., Inoue, T., Ando, J.-i., Funakoshi, K.-i., 2004. Precise determination of phase relations in pyrolite across the 660 km seismic discontinuity by in situ X-ray diffraction and quench experiments. *Phys. Earth Planet. Inter.* 143–144, 185–199.
- Otsuka, K., McCammon, C.A., Karato, S.-i., 2010. Tetrahedral occupancy of ferric iron in (Mg,Fe)O: implications for point defects in the Earth's lower mantle. *Phys. Earth Planet. Inter.* 180, 179–188. <http://dx.doi.org/10.1016/j.pepi.2009.10.005>.
- Panero, W.R., 2008. Cation disorder in ringwoodite and its effects on wave speeds in the Earth's transition zone. *J. Geophys. Res.* 113. <http://dx.doi.org/10.1029/2008JB005676>.
- Paulson, A., Richards, M.A., 2009. On the resolution of radial viscosity structure in modeling long-wavelength postglacial rebound data. *Geophys. J. Int.* 179 (3), 1516–1526. <http://dx.doi.org/10.1111/j.1365-246X.2009.04362.x>.
- Schmid, D.W., Abart, R., Podlachikov, Y.Y., Milke, R., 2009. Matrix rheology effects on reaction rim growth II: coupled diffusion and creep model. *J. Metamorph. Geol.* 27, 83–91.
- Schneider, C.A., Rasband, W.S., Eliceiri, K.W., 2012. NIH Image to ImageJ: 25 years of image analysis. *Nat. Methods* 9, 671–675.
- Shimojuku, A., Kubo, T., Ohtani, E., Nakamura, T., Okazaki, R., Dohmen, R., Chakraborty, S., 2009. Si and O diffusion in (Mg,Fe) $_2$ SiO $_4$  wadsleyite and ringwoodite and its implications for the rheology of the mantle transition zone. *Earth Planet. Sci. Lett.* 284, 103–112.
- Shimojuku, A., Boujibar, A., Yamazaki, D., Yoshino, T., Tomioka, N., Xu, J., 2014. Growth of ringwoodite reaction rims from  $\text{MgSiO}_3$  perovskite and periclase at 22.5 GPa and 1800 °C. *Phys. Chem. Miner.* 41, 555–567. <http://dx.doi.org/10.1007/s00269-014-0669-x>.
- Solomatov, V.S., 1996. Can hotter mantle have a larger viscosity? *Geophys. Res. Lett.* 23, 937–940.
- Solomatov, V.S., El-Khonzondar, R., Tikare, V., 2002. Grain size in the lower mantle: constraints from numerical modeling of grain growth in two-phase systems. *Phys. Earth Planet. Inter.* 129, 265–282.
- Solomatov, V.S., Reese, C.C., 2008. Grain size variations in the Earth's mantle and the evolution of primordial chemical heterogeneities. *J. Geophys. Res.* 113, B07408. <http://dx.doi.org/10.1029/2007JB005319>.
- Sundberg, M., Cooper, R.F., 2008. Crystallographic preferred orientation produced by diffusional creep of harzburgite: effects of chemical interactions among phases during plastic flow. *J. Geophys. Res.* 113, B12208. <http://dx.doi.org/10.1029/2008JB005618>.
- Tammann, G., 1920. Über Anlauffarben von Metallen. *Z. Anorg. Allg. Chem.* 111, 78–89.
- Watson, E.B., Price, J.D., 2002. Kinetics of the reaction  $\text{MgO} + \text{Al}_2\text{O}_3 \rightarrow \text{MgAl}_2\text{O}_4$  and Al–Mg interdiffusion in spinel at 1200 to 2000 °C and 1.0 to 4.0 GPa. *Geochim. Cosmochim. Acta* 66, 2123–2138.
- Wheeler, J., 1992. Importance of pressure solution and coble creep in the deformation of polycrystalline rocks. *J. Geophys. Res.* 97, 4579–4586. <http://dx.doi.org/10.1029/91JB02476>.
- Yamazaki, D., Kato, T., Ohtani, E., Toriumi, M., 1996. Grain growth rates of  $\text{MgSiO}_3$ –perovskite and periclase under lowermantle conditions. *Science* 274, 2052–2054.
- Yamazaki, D., Inoue, T., Okamoto, M., Irifune, T., 2005. Grain growth kinetics of ringwoodite and its implication for rheology of the subducting slab. *Earth Planet. Sci. Lett.* 236, 871–881.
- Yamazaki, D., Yoshino, T., Matsuzaki, T., Katsura, T., Yoneda, A., 2009. Texture of (Mg,Fe)SiO $_3$  perovskite and ferropericlase aggregate: implications for rheology of the lower mantle. *Phys. Earth Planet. Inter.* 174, 138–144. <http://dx.doi.org/10.1016/j.pepi.2008.11.002>.